Supporting Information

Freestanding High-Entropy Phosphide Electrodes for Industrial-Scale Hydrogen Evolution via Far-from-Equilibrium Electrosynthesis

Yunan Wang[1,2], Yapeng Liu*[,3], Pierre Sutra[4], Gaowu Qin[1,5], Song Li*[, 1]

[1] School of Materials Science and Engineering, Northeastern University, Shenyang 110819, China

[2]School of Narcotics Control and Public Order Studies, Criminal Investigation Police University of China, Shenyang, 110854, China

[3] National Key Laboratory of Marine Corrosion and Protection, Luoyang Ship Material Research Institute, Luoyang 471023, China

[4] Laboratoire de Chimie de Coordination, Université de Toulouse, Toulouse, France

[5] Institute for Strategic Materials and Components, Shenyang University of Chemical Technology, Shenyang 110142, China

*Corresponding author. E-mail: liuyp361@163.com (Y Liu); lis@atm.neu.edu.cn (S Li).

Supplementary Experimental Section

Preparation of catalysts

Freestanding hierarchical FeCoNiCuSnP high-entropy phosphides (HEPs) electrodes prepared through a simple electrodeposition process as cathodes under a constant current density of -1.5 A cm^{-2} for 40 s at room temperature with an electrochemical workstation (Zahner iM6e). Typically, a standard three electrode system was employed with Hg/Hg_2SO_4 as the reference electrode, graphite as the counter electrode and the carbon fiber paper (CFP) as the working electrode to be a substrate. Meanwhile, a homogeneous aqueous solution was used as electrolytes involving 0.075 M of $FeCl_2{\cdot}4H_2O$, 0.075 M of $CoCl_2{\cdot}6H_2O$, 0.15 M of $NiCl_2{\cdot}6H_2O$, 0.021 M of $CuCl_2{\cdot}2H_2O$, 0.015 M of $SnCl_2$, 20 mM of NaH_2PO_2 and 0.2 M of HCl to synthesize $Fe_{0.13}Co_{0.26}Ni_{0.14}Cu_{0.31}Sn_{0.12}P_{0.04}$. In addition, FeNiCuSnP, FeCoCuSnP, FeCoNiSnP, FeCoNiCuP and CoNiCuSnP were prepared via the same approach mentioned above except for excluding the according precursor salt for the electrolytes that the sample lacks compared with FeCoNiCuSnP while keeping the total ion concentration unchanged. Besides, FeCoNiCuSn HEAs were prepared via the same approach mentioned above except for excluding the NaH_2PO_2.

Characterization of catalysts

The X-ray diffraction patterns (XRD) were obtained with a Rigaku-D/max 2500 V X-ray diffractometer with Cu Kα radiation (λ = 1.5418 Å). The morphologies of the catalysts were observed by field emission scanning electron microscopy (FE-SEM, JEOL JEM-2100F at 30 kV). The microstructures and element distributions of the catalysts were measured by transmission scanning electron microscopy (TEM, JEOL JEM-200CT at 200 kV) coupled with

selected area electron diffraction (SAED) as well as EDS. X-ray photoelectron spectroscopy (XPS) analysis was performed on a Thermo ESCALAB 250 electron spectrometer using Al Kα X-rays.

Electrochemical measurements

The electrochemical catalytic performance throughout this work was conducted in a N_2-saturated 1.0 M KOH solution using a standard three-electrode electrochemical station (Zahner iM6e) consisting of a catalyst as the working electrode, a graphite rod as the counter electrode, and a Hg/HgO electrode as the reference. All potentials in this work were calibrated with a reversible hydrogen electrode (E vs. RHE) according to the Nernst equation. The as-prepared HEPs were directly used as the working electrodes followed by washing with deionized water to remove the residual electrolytes. For 20 wt.% Pt/C electrodes, 5 mg of the samples and 5 μL of 5% Nafion solution were placed in a 1 mL mixture of water/ethanol with a volume ratio of 3:1 and dispersed by ultrasonication for at least 30 min to form a homogeneous ink. Then, 5 μL of this ink was carefully dropped onto a glassy carbon electrode (GCE) with a diameter of 3 mm and dried in air atmosphere. Linear sweep voltammetry (LSV) was conducted with a scan rate of 5 mV s^{-1}. All polarization curves were automatically corrected by 85% *iR* compensation for ohmic losses arising from active materials, substrate, and solution resistances. A series of cyclic voltammetry (CV) measurements were carried out at sweep rates of 5 ~ 50 mV s^{-1} at nonfaradaic overpotentials to demonstrate the current charging and discharging capacitance for estimating the double-layer capacitance (C_{dl}). The electrochemical surface area (ECSA) value was obtained according to the equation ECSA = C_{dl}/C_s, where C_{dl} is the measured double-layer capacitance and C_s is the specific capacitance. In this work, we assumed a C_s value of 0.04 mF

cm^{-2} according to the literature[1]. The turnover frequency (TOF) value of the reaction was calculated by the equation $TOF=(j \times A_{geo})/(n \times F \times N_{site})$, where j is the current density at an overpotential of 0.206 V vs. RHE, A_{geo} is the geometric area of the electrode, n is the number of electrons involved (2 for HER), F is the Faraday constant, and N_{site} is the total number of metal sites (moles) on the electrode determined by EDS. Electrochemical impedance spectroscopy (EIS) was carried out from 0.1 to 10^5 Hz at a constant potential of -100 mV vs. RHE. The stability measurement was carried out at a static potential of -190 mV vs. RHE with an initial current density of 1 A cm^{-2} by a chronoamperometry method.

DFT calculations

DFT calculations were using the projector-augmented-wave (PAW) potentials with Perdew-Burke-Ernzerhof (PBE) of exchange-correlation interactions as implemented in the Vienna Ab initio Simulation Package (VASP) code. The projected augmented wave (PAW) potentials to describe the ionic cores and take valence electrons into account using a plane wave basis set with a kinetic energy cutoff of 500 eV. Partial occupancies of the Kohn-Sham orbitals were allowed using the Gaussian smearing method and a width of 0.05 eV. The electronic energy was considered self-consistent when the energy change was smaller than 10^{-5} eV. A geometry optimization was considered convergent when the force change was smaller than -0.05 eV/Å. Grimme's DFT-D3 methodology was used to describe the dispersion interactions. The Brillourin zone was sampled with a gamma-centered grid 3×3×1 for FeCoNiCuSn and FeCoNiCuSnP through all the computational process. The increased kpoints of 6×6×2 was used to analysis electronic structure, respectively. In addition, the materials studio was used to aid model construction. The VASPKIT package was employed to aid in the analysis of electronic

structure.

The change in Gibbs free energy at each step was calculated based on the following equation:

$$\Delta G = \Delta E + \Delta ZPE - T\Delta S$$

where ΔE belongs to the reaction energy obtained by the total energy difference between the reactant and product molecules absorbed on the catalyst surface, ΔZPE represents the correction of zero-point energy, T refers to the temperature (298.15 K) and ΔS is the entropy change.

Supplementary Figures

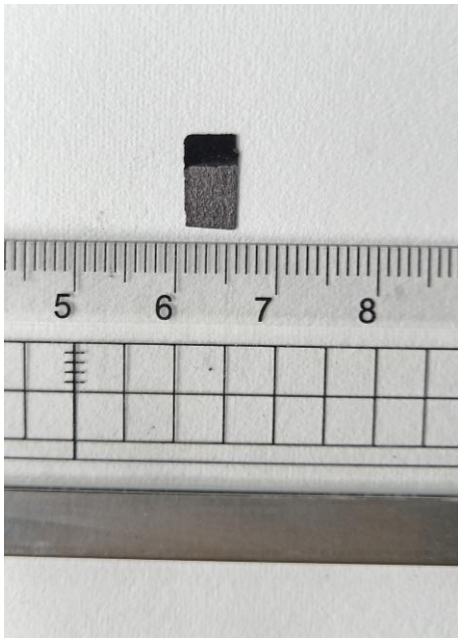

Fig. S1 Photograph of the as-prepared freestanding FeCoNiCuSnP HEP electrodes.

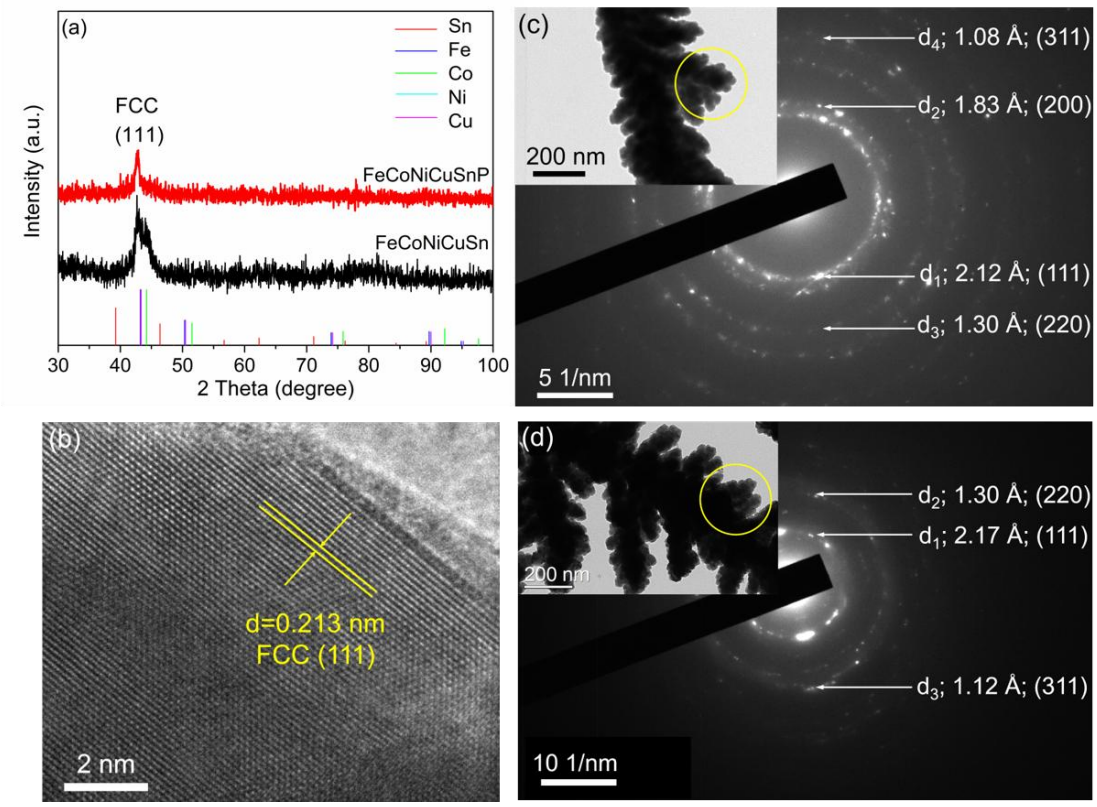

Fig. S2 (a) XRD images of FeCoNiCuSn and FeCoNiCuSnP, respectively. (b) HR-TEM analysis of FeCoNiCuSnP HEPs. (c) SAED results of FeCoNiCuSnP HEPs. (d) SAED results of FeCoNiCuSn.

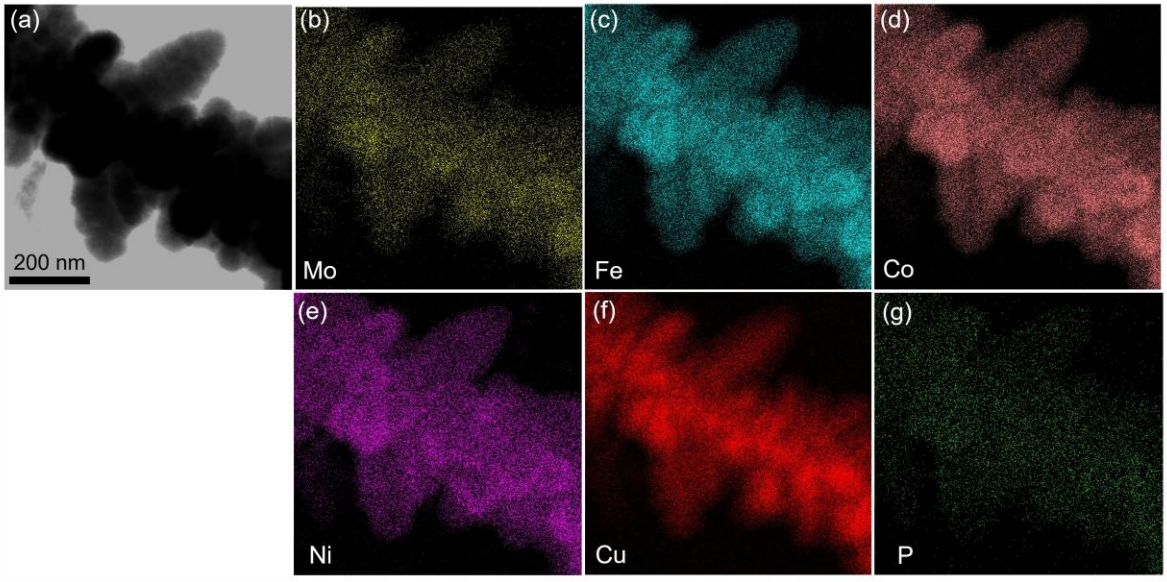

Fig. S3 Morphology and elemental distribution of the senary FeCoNiCrCuMoP HEPs. (a) STEM bright field (BF) image (the inset shows the SAED image.) and (b-h) EDS mapping of Mo, Fe, Co, Ni, Cu, and P, respectively.

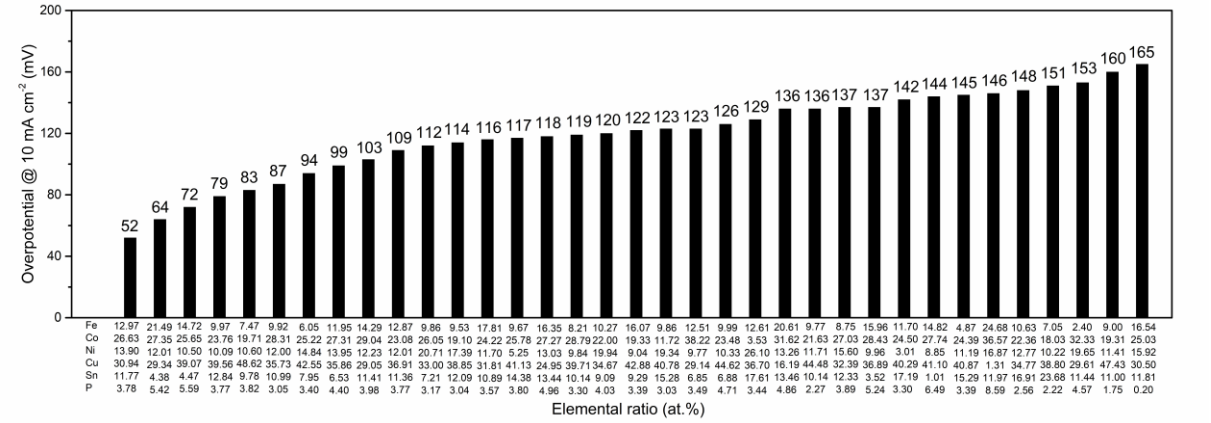

Fig. S4 Comparison of the overpotentials at 10 mA cm^{-2} for samples with different elemental ratios consisting of 5 metals for HER performed in 1.0 M KOH alkaline conditions.

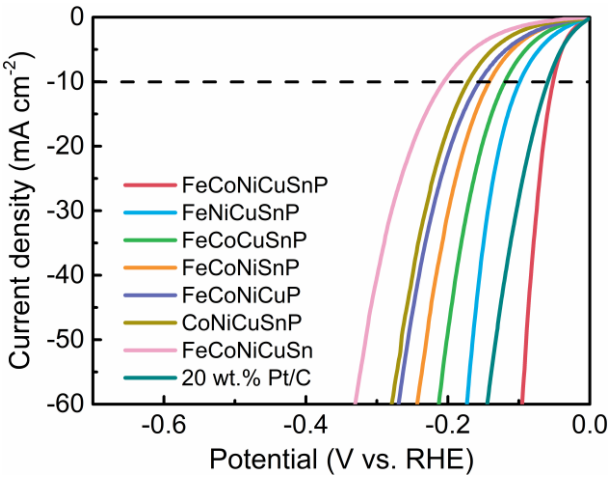

Fig. S5 LSV curves with *iR* loss correction of different samples for HER performed in 1.0 M KOH alkaline conditions.

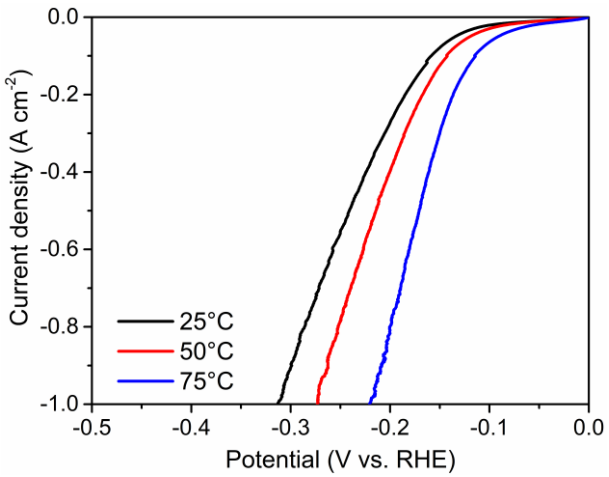

Fig. S6 LSV curves with *iR* loss correction of HEP-α for HER performed in 1.0 M KOH alkaline conditions at different temperatures.

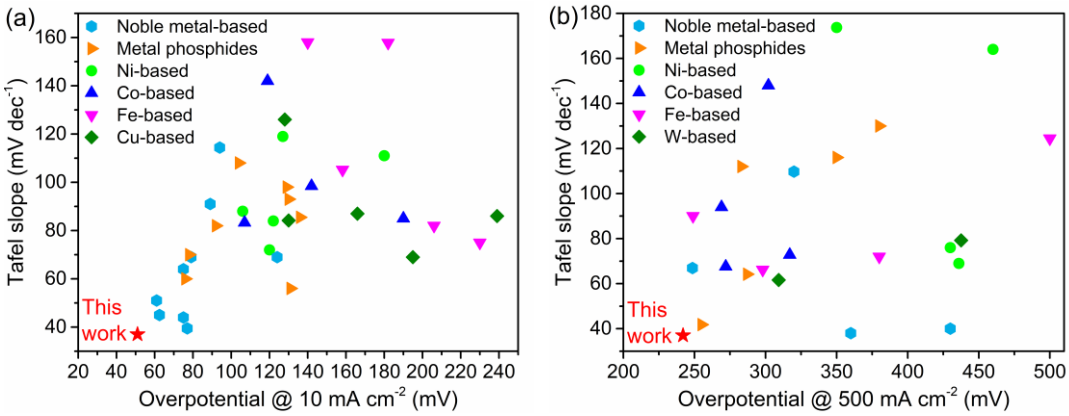

Fig. S7 Comparison of the overpotentials at (a) 10 mA cm^{-2}, (b) 500 mA cm^{-2}, respectively, and the Tafel slopes for different materials for HER performed in 1.0 M KOH alkaline conditions. (The specific sample names and references are listed in Supplementary Table S1 and S2.)

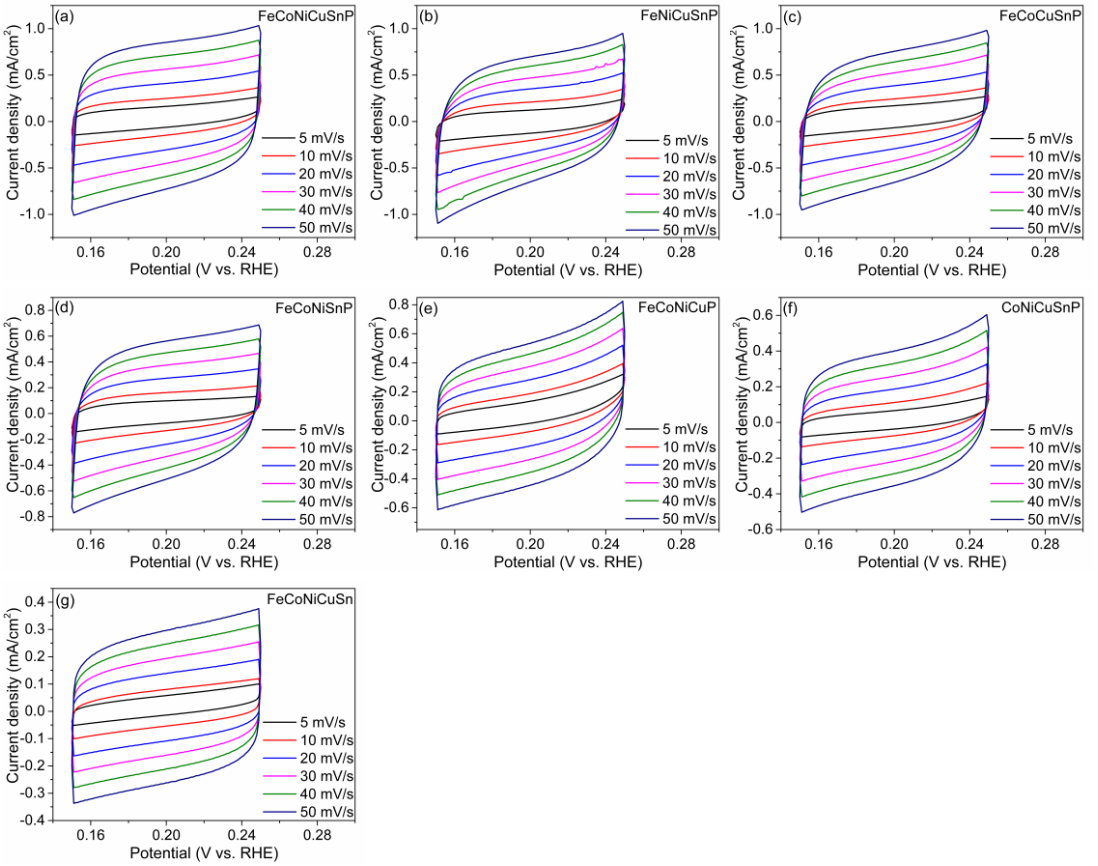

Fig. S8 Cyclic voltammetry (CV) curves at various scan rates in the region of 0.15 to 0.25 V (vs. RHE) for different samples. The double-layer capacitance (C_{dl}) of samples was estimated on the basis of the CV curves through the capacitive currents plotted against the scan rate at 0.2 V (vs. RHE) without faradaic process, which has been universally considered to be linearly proportional to the electrochemical surface area (ECSA).

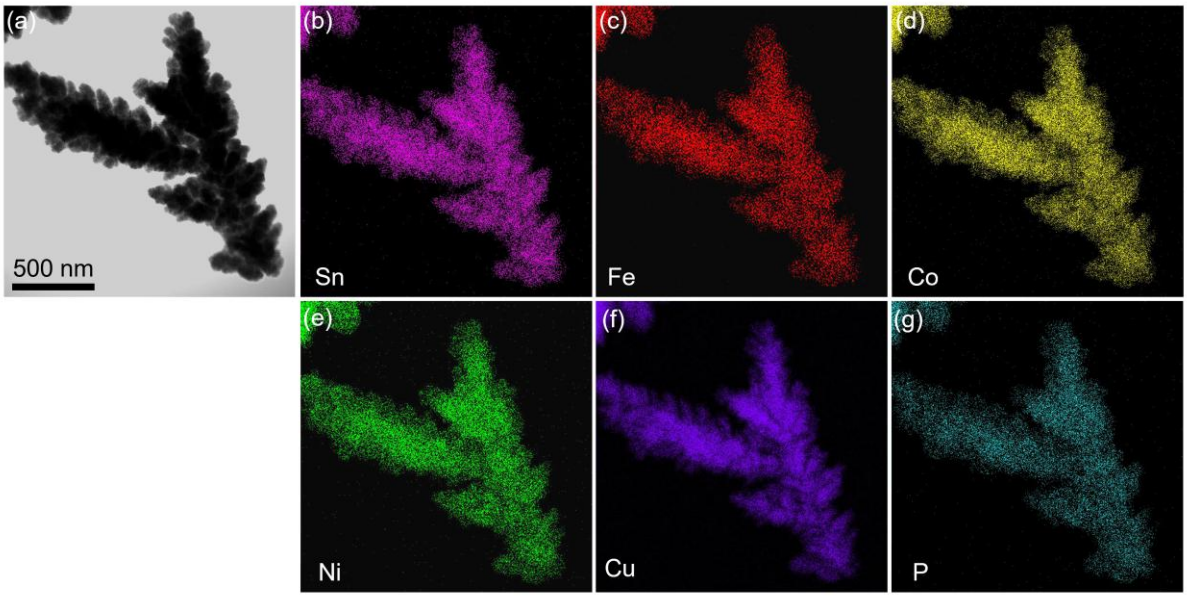

Fig. S9. Elemental distribution of HEP-α collected after stability tests. (a) STEM bright field (BF) image and (b-f) EDS mapping of Sn, Fe, Co, Ni, Cu and P, respectively.

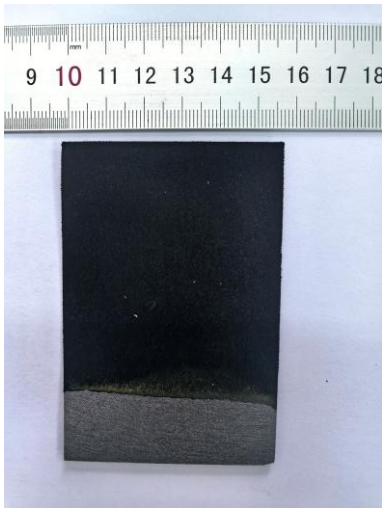

Fig. S10 Photograph of the as-prepared large freestanding FeCoNiCuSnP HEP electrodes.

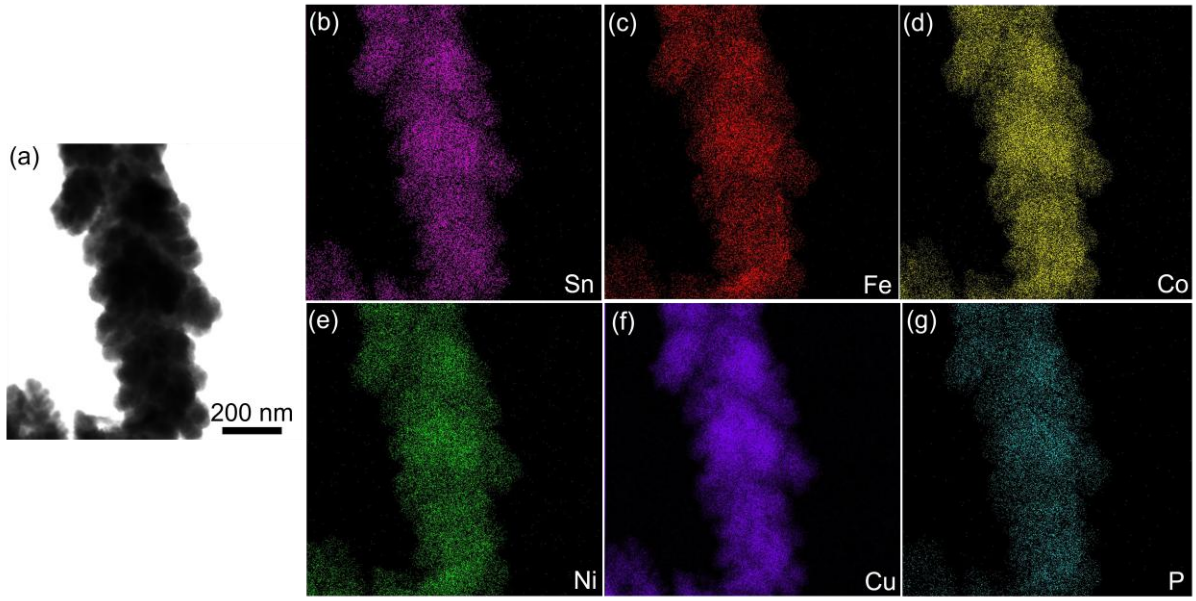

Fig. S11. Elemental distribution of large FeCoNiCuSnP HEP electrodes. (a) STEM bright field (BF) image and (b-f) EDS mapping of Sn, Fe, Co, Ni, Cu and P, respectively.

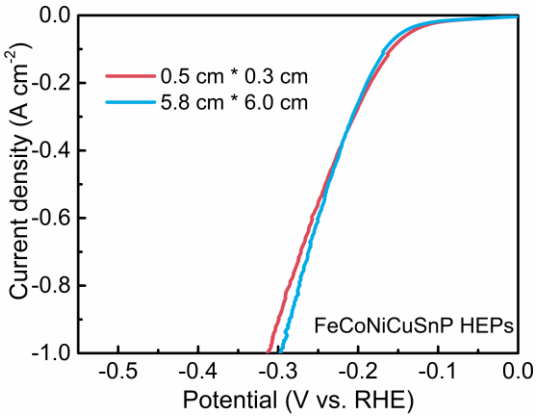

Fig. S12 Comparison of LSV curves with *iR* loss correction of samples with different sizes prepared by far-from-equilibrium electrosynthesis.

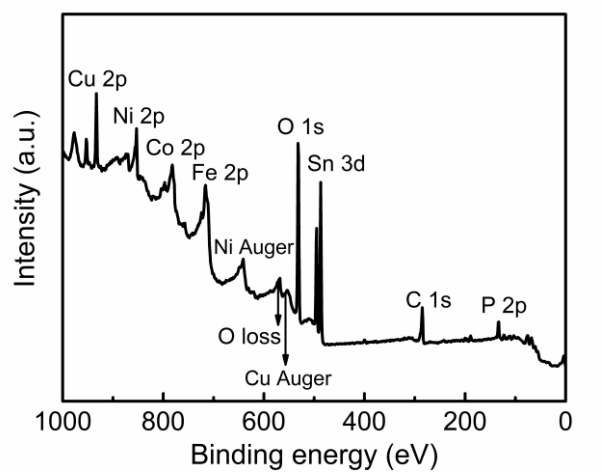

Fig. S13 XPS survey spectrum of FeCoNiCuSnP HEPs.

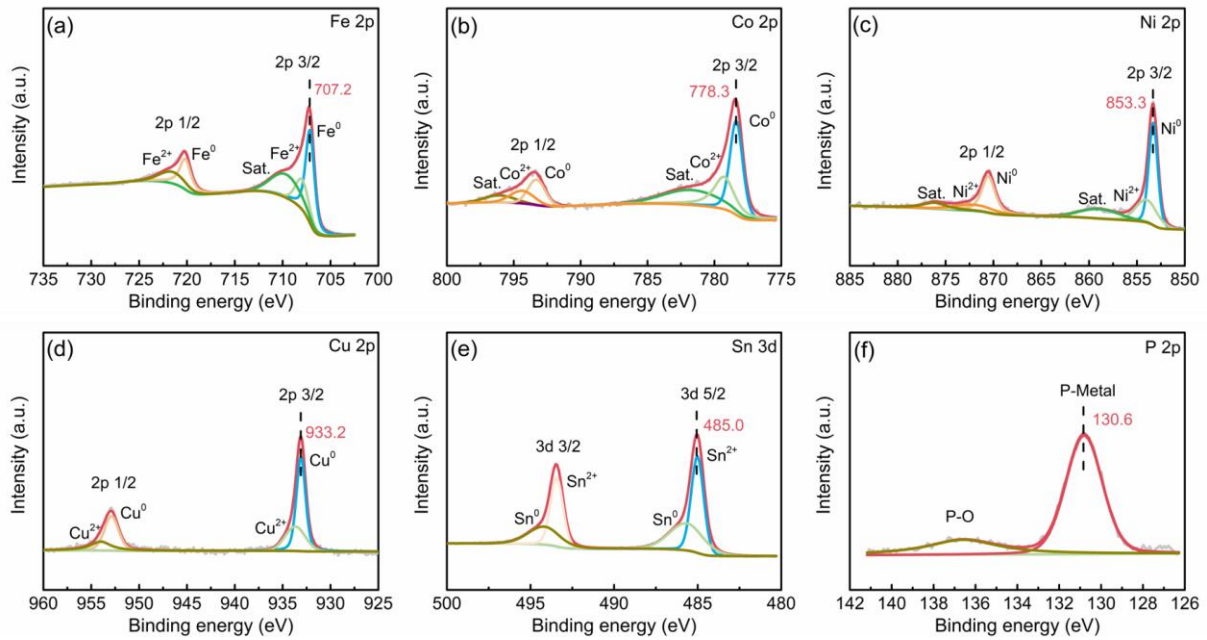

Fig. S14. XPS spectra of FeCoNiCuSnP HEPs reclaimed after 5000 CV cycles. (a) Fe 2p, (b) Co 2p, (c) Ni 2p, (d) Cu 2p, (e) Sn 3d, and (f) P 2p orbitals.

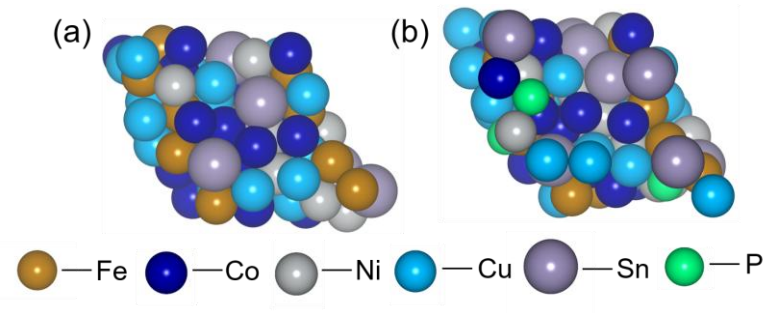

Fig. S15. Models of samples constructed for DFT calculations. (a) FeCoNiCuSn, and (b) FeCoNiCuSnP.

Supplementary Tables

Table S1. The atomic percentage of constituent metals in FeCoNiCuSnP HEPs.

Element	Atomic percentage (at.%)
Fe	13.0
Co	26.6
Ni	13.9
Cu	30.9
Sn	11.8
P	3.8

Table S2. Comparison of the overpotentials at 10 mA cm^{-2} and the Tafel slopes for different materials for HER in 1.0 M KOH alkaline conditions.

Catalysts	Overpotential (mV)	Tafel slope (mV dec^{-1})	Ref.
FeCoNiCuSnP	52	37	This work
$Ni(OH)_2$@Ni/CP	106	88	[3]
Ni/NiO/C-500	127	119	[4]
Ni_3Sn	122	84	[5]
Ni nanoparticle	180	111	[6]
Ni/$CePO_4$	120	72	[7]
c-$CoSe_2$/CC	190	85	[8]
$Co(PO_3)_2$@NPC/MoS_2	119	142	[9]
N-C/Co/Mo_2C	142	98.45	[10]
TiO/Co-S	107	83.3	[11]
Fe-Co-MOFs	182	157.8	[12]
Fe-C_3N_4-TU	206	82	[13]
MoS_2@Fe/Ni-MOF_{600}-3	140	158	[14]
P_{30}-doped Fe/NF	158.17	105.2	[15]
Fe-doped CoP	230	75	[16]
Cu/Ni_3S_2/NF	130	84.19	[17]
Cu/$Ti_3C_2T_x$	128	126	[18]
CuO@NH_2-UiO-66	166	87	[19]
Cu_2Se@NiFe-LDHNS	195	69	[20]
$NiCu_{0.57}/Ni_3S_2$/TM	239	86	[21]
RuO_2/Co_3O_4	89	91	[22]
Ru/C_3N_4/C	79	69	[23]
Pt/VS_2/CP	77	39.46	[24]
$Pt_3Bi_2S_2$	61	51	[25]
Pt/Co_2P/Ni_2P/NF	75	64	[26]
Pd/CeO_2/N, S-rGO	75	44	[27]
Pd-TiN NSs	62.5	45	[28]
Pd–NPs	94	114.38	[29]
AlMnYNiCoAu	124	69	[30]
Mo-Ni-CoP-3	76	60	[31]
NiCoFeP	131	56	[32]
NiCoP	130	93	[33]
Al-Ni_2P/TM	129	98	[34]
$Ni_{1.8}Cu_{0.2}$-P	78	70	[35]
CoP_3@Cu/Cu	92	82	[36]
CoFeNiP/NF	104	108	[37]
FeCoNiCrMn HEMP	136	85.5	[38]

Table S3. Comparison of the overpotentials at 500 mA cm^{-2} and the Tafel slopes for different materials for HER in 1.0 M KOH alkaline conditions.

Catalysts	Overpotential (mV)	Tafel slope (mV dec^{-1})	Ref.
FeCoNiCuSnP	242	37	This work
Pt/C@CC	520.4	49.5	[39]
Pt/C/NF	360	32	[40]
IrFe/NC	430	30	[41]
Ni_3N/Pt	280	36.5	[42]
IrNi-$FeNi_3$/NF	248.6	66.95	[43]
IrNi/NF	320	109.76	[43]
MnO_x/NiFeP/NF	255	41.8	[44]
$Ni_{12}P_5$-$Ni_4Nb_5P_4$/PCC	287	64.2	[45]
$NiCo_{(nf)}$-P	283	112	[46]
$NiCo_{(NS)}$-P	350	116	[46]
$NiCo_{(NR)}$-P	380	130	[46]
N-MoO_2/Ni_3S_2/NF	430	76	[47]
NiFe-LDH/NF	460	164	[40]
Ni-V_2O_3/NF	350	173.71	[48]
Ni/NF	460	240.2	[48]
$NiTe_2$ NWs	436	69	[49]
NiCo	302	148	[50]
$CoMoS_x$/NF	269	94	[51]
CoP_3-Nb_2P	317	72.8	[52]
Co-N-C	272	67.6	[53]
Co_9S_8-hcp	530	99.2	[54]
Fe@Co_9S_8-hcp	298	66.2	[54]
$SnFeS_xO_y$/NF	249	90	[55]
FeS_xO_y/NF	380	72	[55]
$FeNi_3$/NF	500	124.47	[43]
Mo_2C@CC	578.5	91.1	[39]
WC@CC	437.6	79.2	[39]
WC-Mo_2C@CC	309.3	61.6	[39]

Table S4. The specific values of the corresponding parameters achieved from the equivalent circuit for different samples.

Catalysts	R_s (ohm)	R_{CT} (ohm)	*CPE*-T (a.u.)	*CPE*-P (a.u.)
FeCoNiCuSnP	3.59	13.72	0.0943	0.83
FeNiCuSnP	3.32	37.68	0.0568	0.87
FeCoCuSnP	3.17	41.57	0.0696	0.82
FeCoNiSnP	3.24	49.56	0.0634	0.84
FeCoNiCuP	3.86	92.38	0.0947	0.79
CoNiCuSnP	4.61	106.00	0.1042	0.80
FeCoNiCuSn	2.46	290.50	0.0215	0.86

Reference

(1) Li, R.; Liu, X.; Wu, R.; Wang, J.; Li, Z.; Chan, K. C.; Wang, H.; Wu, Y.; Lu, Z. Flexible Honeycombed Nanoporous/glassy Hybrid for Efficient Electrocatalytic Hydrogen Generation. *Adv. Mater.* **2019**, *31* (49), 1904989.

(2) Liu, M.; Min, K. A.; Han, B.; Lee, L. Y. S. Interfacing or Doping? Role of Ce in Highly Promoted Water Oxidation of NiFe-Layered Double Hydroxide. *Adv. Energy Mater.* **2021**, *11* (33), 213824.

(3) Lu, S.; Zhao, B.; Chen, M.; Wang, L.; Fu, X. Z.; Luo, J. L. Electrodeposited Porous Spherical $Ni(OH)_2$@Ni on Carbon Paper for High-Efficiency Hydrogen Evolution. *Int. J. Hydrogen Energy* **2021**, *46* (2), 1540–1547.

(4) Yan, Y.; Ma, Q.; Cui, F.; Zhang, J.; Cui, T. Carbon Onions Coated Ni/NiO Nanoparticles as Catalysts for Alkaline Hydrogen Evolution Reaction. *Electrochim. Acta* **2022**, *430*, 141090.

(5) Zhang, D.; Ji, S. J.; Cao, Y.; Suen, N. T. Exploring the Synergistic Effect of Alloying toward Hydrogen Evolution Reaction: A Case Study of Ni3M (M = Ti, Ge and Sn) Series. *Dalt. Trans.* **2022**, *51* (25), 9728–9734.

(6) Abbas, S. A.; Iqbal, M. I.; Kim, S. H.; Jung, K. D. Catalytic Activity of Urchin-like Ni Nanoparticles Prepared by Solvothermal Method for Hydrogen Evolution Reaction in Alkaline Solution. *Electrochim. Acta* **2017**, *227*, 382–390.

(7) Ke, H.; Wang, J.; Yu, N.; Pu, Y.; Tan, J.; Gong, M.; Zhang, W.; Xue, Y.; Yu, F. Interface-Engineered Ni/$CePO_4$ Heterostuctures for Efficient Electro-/photo-Catalytic Hydrogen Evolution. *Fuel* **2023**, *344*, 127971.

(8) Chen, P.; Xu, K.; Tao, S.; Zhou, T.; Tong, Y.; Ding, H.; Zhang, L.; Chu, W.; Wu, C.; Xie, Y. Phase-Transformation Engineering in Cobalt Diselenide Realizing Enhanced Catalytic Activity for Hydrogen Evolution in an Alkaline Medium. *Adv. Mater.* **2016**, *28* (34), 7527–7532.

(9) Zheng, H. B.; Li, Y. L.; Wang, Y. L.; Ma, F.; Gao, P. Z.; Guo, W. M.; Qin, H.; Liu, X. P.; Xiao, H. N. Fabrication of $Co(PO_3)_2$@NPC/MoS_2 Heterostructures for Enhanced Electrocatalytic Hydrogen Evolution. *J. Alloys Compd.* **2022**, *894*, 162411.

(10) Chen, L. F.; Hou, C. C.; Zou, L.; Kitta, M.; Xu, Q. Uniformly Bimetal-Decorated Holey Carbon Nanorods Derived from Metal−organic Framework for Efficient Hydrogen Evolution. *Sci. Bull.* **2021**, *66* (2), 170–178.

(11) Zhang, B.; Zhou, Y.; Cao, Y.; Wang, X.; Zhang, K.; Tu, J.; Ding, L. Enhancing Hydrogen Evolution by Optimizing the Hydrogen Adsorption on Titanium Monoxide Nanodot-Decorated Cobalt Sulfide Nanosheets. *ChemPhysChem* **2022**, *23* (3), 24-29.

(12) Tan, W.; Xie, S.; Yang, J.; Lv, J.; Yin, J.; Zhang, C.; Wang, J.; Shen, X.; Zhao, M.; Zhang, M.; He, G.; Yang, L. Effect of Carbonization Temperature on Electrocatalytic Water Splitting of Fe-Co Anchored on N-Doped Porous Carbon. *J. Solid State Chem.* **2021**, *302*, 122435.

(13) Wang, H.; Sun, P.; Jiang, H.; Li, X.; Ma, X.; Shao, K.; Wang, C. Fe-Doped Porous g-C_3N_4: An Efficient Electrocatalyst with Fe-N Active Sites for Electrocatalytic Hydrogen Evolution Reaction under Alkaline Conditions. *ChemistrySelect* **2022**, *7* (21), e202200306.

(14) Lin, Z.; Feng, T.; Ma, X.; Liu, G. Fe/Ni Bi-Metallic Organic Framework Supported 1T/2H MoS_2 Heterostructures as Efficient Bifunctional Electrocatalysts for Hydrogen and Oxygen Evolution. *Fuel* **2023**, *339*, 127395.

(15) Ju, Y.; Feng, S.; Wang, X.; Li, M.; Wang, L.; Xu, R.; Wang, J. Facile Preparation of a Porous Nanosheet PX-Doped Fe Bi-Functional Catalyst with Excellent OER and HER Electrocatalytic Activity. *ChemistrySelect* **2021**, *6* (20), 4979–4990.

(16) Tang, C.; Zhang, R.; Lu, W.; He, L.; Jiang, X.; Asiri, A. M.; Sun, X. Fe-Doped CoP Nanoarray: A Monolithic Multifunctional Catalyst for Highly Efficient Hydrogen Generation. *Adv. Mater.* **2017**, *29* (2), 1602441.

(17) Xiao, Q.; Xu, X.; Fan, C.; Qi, Z.; Jiang, S.; Deng, Q.; Tong, Q.; Zhang, Q. Deposition of Cu on Ni_3S_2 Nanomembranes with Simply Spontaneous Replacement Reaction for Enhanced Hydrogen Evolution Reaction. *J. Electroanal. Chem.* **2022**, *911*, 116214.

(18) Wang, B.; Shu, Q.; Chen, H.; Xing, X.; Wu, Q.; Zhang, L. Copper-Decorated $Ti_3C_2T_x$ MXene Electrocatalyst for Hydrogen Evolution Reaction. **2022**, *12*, 2022.

(19) Fiaz, M.; Athar, M. Enhancing the Hydrogen and Oxygen Evolution Reaction Efficiency of Amine Functionalized MOF NH_2-UiO-66 via Incorporation of CuO Nanoparticles. *Catal. Letters* **2020**, *150* (11), 3314–3326.

(20) Qi, H.; Zhang, P.; Wang, H.; Cui, Y.; Liu, X.; She, X.; Wen, Y.; Zhan, T. Cu2Se Nanowires Shelled with NiFe Layered Double Hydroxide Nanosheets for Overall Water-Splitting. *J. Colloid Interface Sci.* **2021**, *599*, 370–380.

(21) Wang, J.; Wang, Y.; Yao, Z.; Xie, T.; Deng, Q.; Jiang, Z.; Zhu, Q.; Liu, S.; Peng, Y.; Zhang, X. Enhanced Hydrogen Evolution Activity of Ni/Ni_3S_2 Nanosheet Grown on Ti Mesh by Cu Doped Ni . *J. Electrochem. Soc.* **2019**, *166* (2), 168–173.

(22) Liu, H.; Xia, G.; Zhang, R.; Jiang, P.; Chen, J.; Chen, Q. MOF-Derived RuO_2/Co_3O_4 Heterojunctions as Highly Efficient Bifunctional Electrocatalysts for HER and OER in Alkaline Solutions. *RSC Adv.* **2017**, *7* (7), 3686–3694.

(23) Zheng, Y.; Jiao, Y.; Zhu, Y.; Li, L. H.; Han, Y.; Chen, Y.; Jaroniec, M.; Qiao, S. Z. High Electrocatalytic Hydrogen Evolution Activity of an Anomalous Ruthenium Catalyst. *J. Am. Chem. Soc.* **2016**, *138* (49), 16174–16181.

(24) Zhu, J.; Cai, L.; Yin, X.; Wang, Z.; Zhang, L.; Ma, H.; Ke, Y.; Du, Y.; Xi, S.; Wee, A. T. S.; Chai, Y.; Zhang, W. Enhanced Electrocatalytic Hydrogen Evolution Activity in Single-Atom Pt-Decorated VS2 Nanosheets. *ACS Nano* **2020**, *14* (5), 5600–5608.

(25) Fang, Y.; Wang, S.; Lin, G.; Wang, X.; Huang, F. A New Compound $Pt_3Bi_2S_2$ with Superior Performance for the Hydrogen Evolution Reaction. *Chem. Commun.* **2021**, *57* (64), 7946–7949.

(26) Xiao, X.; Sun, D.; Liu, X.; Qiu, B.; Xu, X.; Zhang, D.; Yang, T. Ultra-Low Amount Pt-Doped Co_2P/Ni_2P on Nickel Foam as an Efficient Electrocatalyst for the Hydrogen Evolution Reaction in an Alkaline Electrolyte. *Sustain. Energy Fuels* **2021**, *5* (4), 1059–1066.

(27) Woldetinsay, M.; Soreta, T. R.; Palani, K.; Maiyalagan, T.; Olu, F. E. Synthesis, Characterization and Electrocatalytic Study of Pd Supported on CeO_2–N, S-rGO Composite towards Hydrogen and Oxygen Evolution Reaction. *J. Mater. Sci. Mater. Electron.* **2021**, *32* (9), 12241–12252.

(28) Anandha Babu, G.; Navaneethan, M. Superficial Interface of Pd-Dispersed Titanium Nitride Electrocatalysts for Hydrogen Evolution Reaction. *Mater. Lett.* **2022**, *325*, 132843.

(29) Limaye, A. S.; Alsaiari, M.; Shinde, P. V.; Ghosh, A.; Jalalah, M.; Rout, C. S.; Patil, S. a.; Harraz, F. a.; Dateer, R. B. Greener Approach for Pd–NPs Synthesis Using Mangifera Indica Leaf Extract: Heterogeneous Nano Catalyst for Direct C–H Arylation of (Poly)Fluorobenzene, Hiyama Coupling Reaction and Hydrogen Evolution Reaction Study. *Catal. Letters* **2022**, *153* (7), 1988-2004.

(30) Zou, P.; Zang, B.; Song, L.; Xu, W.; Huo, J.; Wang, J. Q. Nanoporous AlMnYNiCoAu Catalysts for Hydrogen Evolution. *ACS Appl. Nano Mater.* **2022**, *5* (12), 17673–17681.

(31) Lin, J.; Yan, Y.; Li, C.; Si, X.; Wang, H.; Qi, J.; Cao, J.; Zhong, Z.; Fei, W.; Feng, J. Bifunctional Electrocatalysts Based on Mo-Doped NiCoP Nanosheet Arrays for Overall Water Splitting. *Nano-Micro Lett.* **2019**, *11* (1), 55.

(32) Guo, Y.; Tang, J.; Wang, Z.; Sugahara, Y.; Yamauchi, Y. Hollow Porous Heterometallic Phosphide Nanocubes for Enhanced Electrochemical Water Splitting. *Small* **2018**, *14* (44), 1802442.

(33) Zhou, Q.; Wang, D. 3D Nanoporous NiCoP as a Highly Efficient Electrocatalyst for the Hydrogen Evolution Reaction in Alkaline Electrolyte. *New J. Chem.* **2022**, *46* (16), 7490–7496.

(34) Du, H.; Xia, L.; Zhu, S.; Qu, F.; Qu, F. Al-Doped Ni2P Nanosheet Array: A Superior and Durable Electrocatalyst for Alkaline Hydrogen Evolution. *Chem. Commun.* **2018**, *54* (23), 2894–2897.

(35) Chu, S.; Chen, W.; Chen, G.; Huang, J.; Zhang, R.; Song, C.; Wang, X.; Li, C.; Ostrikov, K. (Ken). Holey Ni-Cu Phosphide Nanosheets as a Highly Efficient and Stable Electrocatalyst for Hydrogen Evolution. *Appl. Catal. B Environ.* **2019**, *243*, 537–545.

(36) Hou, M.; Xu, Y.; Li, X.; Dong, Y.; Sun, F.; Tang, D.; Cai, M.; Jin, C.; Dong, Y.; Qu, D.; Xie, Z.; Lin, Y.; Zhang, C. Coralline-like CoP_3@Cu as an Efficient Electrocatalyst for the Hydrogen Evolution Reaction in Acidic and Alkaline Solutions. *New J. Chem.* **2020**, *44* (43), 18601–18607.

(37) Wang, M.; Chen, Y.; Li, T. Controllable Preparation of Nickel Phosphide Using Iron and Cobalt as Electrocatalyst for Hydrogen Evolution Reaction in Alkaline Media. *Mater. Today Chem.* **2022**, *24*, 100914.

(38) Zhao, X.; Xue, Z.; Chen, W.; Wang, Y.; Mu, T. Eutectic Synthesis of High-Entropy Metal Phosphides for Electrocatalytic Water Splitting. *ChemSusChem* **2020**, *13* (8), 2038–2042.

(39) Liu, W.; Wang, X.; Qu, J.; Ma, Y.; Liu, X.; Kuai, C.; Guo, Y.; Yin, H.; Wang, D. Computation-Guided Design and Preparation of Durable and Efficient WC-Mo2C Heterojunction for Hydrogen Evolution Reaction. *Cell Reports Phys. Sci.* **2022**, *3* (3), 100784.

(40) Yu, M.; Wang, Z.; Liu, J.; Sun, F.; Yang, P.; Qiu, J. A Hierarchically Porous and Hydrophilic 3D nickel–iron/MXene Electrode for Accelerating Oxygen and Hydrogen Evolution at High Current Densities. *Nano Energy* **2019**, *63*, 103880.

(41) Jiang, P.; Huang, H.; Diao, J.; Gong, S.; Chen, S.; Lu, J.; Wang, C.; Sun, Z.; Xia, G.; Yang, K.; Yang, Y.; Wei, L.; Chen, Q. Improving Electrocatalytic Activity of Iridium for Hydrogen Evolution at High Current Densities above 1000 mA cm^{-2}. *Appl. Catal. B Environ.* **2019**, *258*, 117965.

(42) Wang, Y.; Chen, L.; Yu, X.; Wang, Y.; Zheng, G. Superb Alkaline Hydrogen Evolution and Simultaneous Electricity Generation by Pt-Decorated Ni_3N Nanosheets. *Adv. Energy Mater.* **2017**, *7* (2), 1601390.

(43) Wang, Y.; Qian, G.; Xu, Q.; Zhang, H.; Shen, F.; Luo, L.; Yin, S. Industrially Promising IrNi-$FeNi_3$ Hybrid Nanosheets for Overall Water Splitting Catalysis at Large Current Density. *Appl. Catal. B Environ.* **2021**, *286*, 119881.

(44) Wang, P.; Luo, Y.; Zhang, G.; Wu, M.; Chen, Z.; Sun, S.; Shi, Z. MnOx-Decorated Nickel-Iron Phosphides Nanosheets: Interface Modifications for Robust Overall Water Splitting at Ultra-High Current Densities. *Small* **2022**, *18* (7), 2105803.

(45) Chen, D.; Xu, Z.; Chen, W.; Chen, G.; Huang, J.; Song, C.; Zheng, K.; Zhang, Z.; Hu, X.; Choi, H. S.; Ostrikov, K. Mulberry-Inspired Nickel-Niobium Phosphide on Plasma-Defect-Engineered Carbon Support for High-Performance Hydrogen Evolution. *Small* **2020**, *16* (43), 2004843.

(46) Xu, Z.; Yeh, C. L.; Chen, J. L.; Lin, J. T.; Ho, K. C.; Lin, R. Y. Y. Metal-Organic Framework-Derived 2D NiCoP Nanoflakes from Layered Double Hydroxide Nanosheets for Efficient Electrocatalytic Water Splitting at High Current Densities. *ACS Sustain. Chem. Eng.* **2022**, *10* (35), 11577-11586.

(47) Wang, L.; Cao, J.; Lei, C.; Dai, Q.; Yang, B.; Li, Z.; Zhang, X.; Yuan, C.; Lei, L.; Hou, Y. Strongly Coupled 3D N-Doped MoO_2/Ni_3S_2 Hybrid for High Current Density Hydrogen Evolution Electrocatalysis and Biomass Upgrading. *ACS Appl. Mater. Interfaces* **2019**, *11* (31), 27743–27750.

(48) Qian, G.; Chen, J.; Luo, L.; Zhang, H.; Chen, W.; Gao, Z.; Yin, S.; Tsiakaras, P. Novel Bifunctional V_2O_3 Nanosheets Coupled with N-Doped-Carbon Encapsulated Ni Heterostructure for Enhanced Electrocatalytic Oxidation of Urea-Rich Wastewater. *ACS Appl. Mater. Interfaces* **2020**, *12* (34), 38061–38069.

(49) Anantharaj, S.; Karthick, K.; Kundu, S. NiTe2 Nanowire Outperforms Pt/C in High-Rate Hydrogen Evolution at Extreme pH Conditions. *Inorg. Chem.* **2018**, *57* (6), 3082–3096.

(50) Zhu, W.; Chen, W.; Yu, H.; Zeng, Y.; Ming, F.; Liang, H.; Wang, Z. NiCo/NiCo–OH and NiFe/NiFe–OH Core Shell Nanostructures for Water Splitting Electrocatalysis at Large Currents. *Appl. Catal. B Environ.* **2020**, *278*, 119326.

(51) Shan, X.; Liu, J.; Mu, H.; Xiao, Y.; Mei, B.; Liu, W.; Lin, G.; Jiang, Z.; Wen, L.; Jiang, L. An Engineered Superhydrophilic/Superaerophobic Electrocatalyst Composed of the Supported $CoMoS_x$ Chalcogel for Overall Water Splitting. *Angew. Chem. Int. Ed.* **2020**, *59* (4), 1659–1665.

(52) Xiang, H.; Chen, W.; Li, T.; Huang, J.; Chen, G.; Gong, T.; Ken Ostrikov, K. High-Performance CoNb Phosphide Water Splitting Electrocatalyst on Plasma-Defect-Engineered Carbon Cloth. *Chem. Eng. J.* **2022**, *446*, 137419.

(53) Liu, R.; Gong, Z.; Liu, J.; Dong, J.; Liao, J.; Liu, H.; Huang, H.; Liu, J.; Yan, M.; Huang, K.; Gong, H.; Zhu, J.; Cui, C.; Ye, G.; Fei, H. Design of Aligned Porous Carbon Films with Single-Atom Co–N–C Sites for High-Current-Density Hydrogen Generation. *Adv. Mater.* **2021**, *33* (41), 2103533.

(54) Tian, B.; Sun, L.; Ho, D. Hexagonal Co_9S_8: Experimental and Mechanistic Study of Enhanced Electrocatalytic Hydrogen Evolution of a New Crystallographic Phase. *Adv. Funct. Mater.* **2023**, *33* (19), 2210298.

(55) Zhang, T.; Han, J.; Tang, T.; Sun, J.; Guan, J. Binder-Free Bifunctional SnFe Sulfide/oxyhydroxide Heterostructure Electrocatalysts for Overall Water Splitting. *Int. J. Hydrogen Energy* **2023**, *48* (12), 4594–4602.